quaternary

MDPI

Communication

Geochemistry and Sedimentology of a Minerotrophic Peat in a Western Mediterranean Mountain Wilderness Area

Vladimir Goutiers [1,2] and Christopher Carcaillet [2,3,*]

[1] INRAE–UMR AGIR, 24 Chemin de Borde-Rouge, F-31326 Castanet Tolosan, France
[2] Ecole Pratique des Hautes Etudes (EPHE), Paris Sciences & Lettres Université (PSL), F-75014 Paris, France
[3] Univ Lyon, Université Claude Bernard Lyon 1, CNRS, ENTPE (UMR 5023 LEHNA), F-69622 Villeurbanne, France
* Correspondence: christopher.carcaillet@ephe.psl.eu

Highlights:

- The peat age was late Holocene, and less than 1900 years old.
- The peat contained no charcoal, probably due to the lack of woody cover at the site for 1900 years.
- Depth profiles of clay and nutrients (P, K, Ca, Mg) revealed an increase in atmospheric inputs over time, while nitrogen is homogeneously sequestrated in depth.
- The dominant metallic trace elements (MTE) were cadmium, which peaked during the Roman epoch, then lead and mercury concentrated during the modern period, but decreasing onwards.
- Peat geochemistry is strongly influenced by local and regional human activities, revealing a peat modified by social imprints.

Abstract: Sedimentological and biogeochemical measurements were conducted on minerotrophic peat in a wilderness area on a granitic plateau to reconstruct the local ecosystem's history and clarify the peat's response to local and global changes. The peat is less than 1900 years old. Its clay and iron (Fe) concentration profiles revealed an increasing atmospheric influx over time, whereas the levels of its nutrients (P, K, Ca, Mg) have increased since the 19th century. Additionally, changes in the relative abundance of amorphous aluminium indicated a gradual decrease in soil weathering. The dominant metallic trace elements were cadmium during the Roman epoch and early Middle Ages, then lead and mercury during the modern and the industrial eras. Unexpectedly, the peat proved to be sub-modern and lacks wildfire proxies, probably indicating an absence of nearby woodlands over the last 1900 years. Its concentrations of Ca and Mg indicate that airborne transport of particles released by soil erosion in lowland agricultural plains has strongly affected the peat's composition since the 18th–19th century. The site has also been heavily influenced by metallic contamination due to regional metallurgy and agriculture, producing a peat that has been modified by social imprints over several centuries.

Keywords: aluminium; cadmium; fen; granulometry; iron; lead; mercury; nitrogen; silicon

Citation: Goutiers, V.; Carcaillet, C. Geochemistry and Sedimentology of a Minerotrophic Peat in a Western Mediterranean Mountain Wilderness Area. *Quaternary* **2022**, *5*, 48. https://doi.org/10.3390/quat5040048

Academic Editor: James B. Innes

Received: 18 August 2022
Accepted: 17 November 2022
Published: 21 November 2022

1. Introduction

Efforts to conserve wilderness areas require benchmarks to determine the legacies of historical processes. Globally, ecosystems are shaped by long-term changes in climate (macro-scale process) and social stresses (land use). Land use is a complex and nested set of micro- and macro-scale mechanisms that includes (going from the smallest to the largest scales) anthropogenic stand disturbances, the husbandry habits of local human societies, and the regional influences of civilizations, all of which may have different effects and leave distinct traces in an ecosystem's archive. Studying their proxies provides a valuable way of disentangling their contributions in order to understand the ecosystem's current state.

The present study aimed to characterise the peat composition of a Mediterranean mountain plateau in terms of its granulometry, the geochemistry of aluminium (Al) and iron (Fe), metal trace elements (MTE), and macro-nutrients. Links are assumed between some components, notably the lighter ones whose concentrations may be heavily influenced by atmospheric deposition [1,2]. The ratios of amorphous Al and Fe to the total amounts of the same elements were used as proxies for particle weathering [3], while MTE levels were determined to elucidate the historical contributions of regional industrial activities and mining to the peat's current pollution burden [4–7]. Calcium (Ca) and magnesium (Mg) were used to trace atmospheric inputs [1,8], based on the knowledge that the peat's granitic bedrock is depleted in these elements. The depth profiles of all elements were used in conjunction with radiocarbon measurements of the complete core to unravel the timing of the atmospheric inputs. In addition, macro-charcoal particles were counted along the core's depth profile to reconstruct the peat's wildfire history [9]. Macro-particles (>200 µm) were preferred to micro-particles for this purpose because micro-charcoal is considered to be a proxy of both local and regional burnings, whereas macro-charcoal reflects stand- to local-scale fire history [10–12].

All of the identified temporal patterns are discussed in relation to the site's known land use history over the last 2000 years. Although this region has been used for agriculture since the Neolithic, its agriculture development increased significantly during the 1st century AD [13,14], when local vineyards expanded in association with the establishment of the first Roman Province in Gaul (*Gallia narbonensis*), around the nearby city of Narbonne on the *Via Domitia* (a Roman commercial route) and its antique harbour. The lowland plains between the slopes of the Massif Central and the Mediterranean Sea have deep and productive soils that supported the development of a rich agriculture with a heavy emphasis on grapes and cereals. The historical development of agriculture at the site can be traced, thanks to atmospheric inputs, from the depth profiles of major elements (N, P, K), while the intensity of lowland agriculture on calcareous soils is reflected in the concentrations of Ca and Mg.

There is also extensive archaeological evidence of ore mining in the studied area [15,16], which influenced the accumulation of MTE in regional sediments [17,18] in accordance with the findings of several other studies conducted in southwestern Europe [19,20]. Among the MTE, mercury (Hg) and lead (Pb) are commonly used as proxies of past ore mining [4,6], but the usefulness of cadmium (Cd) as an indicator is disputed: some studies suggest that it is a poor mining proxy due to its high mobility in peat [7], while others conclude that its taphonomy allows accurate tracing of regional mining activity [20–22].

The following text discusses sedimentological and geochemical results in terms of erosion, weathering, or aerial transportation of mineral particles linked to regional land use history. The occurrence of charcoal is discussed in light of the late Holocene inception of the peat and the previously reported effects of tree cover suppression on regional wildfire histories.

2. Materials and Methods

2.1. Study Site

The studied site (43°36′09″ N, 02°58′25″ E) is a headwater peat hollow located at 1052 m above sea level (asl) on the Caroux plateau, which culminates at 1090 m asl in the Espinouse Massif—the southwestern area of France's Massif Central (Figure 1). Because the site is a headwater peat, water transportation of elements and particles can be excluded [23]. The plateau is situated north of the Orb River basin and one of its tributaries (the Jaur river) that drains into the Mediterranean Sea. The Caroux plateau is bordered by the Héric Gorges to the southwest and the Colombières Gorges to the southeast. Narbonne is about 45 km south of the Caroux mountain. This plateau is formed from granitic and metamorphic rocks (gneisses and micaschists) and consequently has acidic superficial soils. It belongs to the geological massif of the Montagne Noire.

Figure 1. Aerial view of the studied site (GoogleEarth image, 2014); the exact location of the coring is indicated by the white asterisk. The inset shows the location of the Caroux plateau in the southwestern Massif Central (map from Wikimedia, used under CC BY-SA).

The site's present day vegetation grows on drained acidic soils lying. It consists mainly of montane heathland resulting from the land's abandonment since the 1950's. The heathland is planted with Scots pine (*Pinus sylvestris* L.), and two introduced pine species, mountain (*P. uncinata* Ramon ex. DC) and black pines (*P. nigra* ssp. *nigra* Arn.). Scattered beeches (*Fagus sylvatica* L.) and white oaks (*Quercus pubescens*) occur with willows (*Salix* sp.), red elderberry (*Sambucus racemosa* L.), and birch (*Betula pendula*). The heathland is dominated by *Calluna vulgaris* (L.) Hull., with *Erica cinearea* L., *Cytisus oromediterraneus* Rivas Mart and *C. scoparius* (L.) Link. In addition, also present are ferns (*Pteridium aquilinum* (L.) Kuhn.), herbs (mainly *Molinia caerulea* (L.) Moench, but also *Carex* spp., *Deschampsia cespitosa* L., *Holcus lanatus* L., and *Juncus acutiflorus* Ehrh. Ex Hoffm.), and forbs (notably *Epilobium angustifolium* L.). The peat vegetation is mostly dominated by *Carex* spp., with hypnaceae (bryophytes), scattered *Sphagnum* sp. Cushions, and *Drosera rotundifolia* L.

2.2. Peat Sampling and Dating

Sediments were collected on July 2007, using a "Russian" stainless steel corer (1000 × 10 cm) in a peated hollow of a few hundred square meters (Figure 1), in the northwestern area of the plateau. The deepest area (90 cm) of the peatland was chosen because it was expected to provide the longest chronology. The low thickness (90 cm) of the peat here is within the range of acidic fen thicknesses in the area [24] and in southwestern Europe [25] more generally. Three parallel cores were collected, one for charcoal and ^{14}C dating, one for granulometry, and one for geochemistry.

Nine AMS ^{14}C measurements were conducted on decomposed plant macroremains of herbs and few bryophytes at the LMC14 lab (Gif-sur-Yvette, France); these measurements were labelled SacA. Radiocarbon ages were calibrated in calendar years using version 8.2 of the CALIB program [26] with the Intcal20 dataset [27]. An age depth model was generated using the package rBacon version 2.5.8 [28] with priors of 20 years/cm^{-1} for the accumulation rate and 1.5 for the curve distribution shape.

2.3. Charcoal Counting for Fire Analyses

To retrieve charcoal, sediment cores were analysed without discontinuity and sliced at 1 cm intervals. Macro-charcoal was extracted from soaked sediment by water sieving through a mesh of 250 µm. It is widely accepted that such charcoal macro-particles are produced locally [10,12]. For charcoal counting, sediments were first deflocculated and bleached with NaClO before sieving under a gentle water spray [9].

2.4. Granulometry and Geochemical Analyses

For the granulometric and geochemical analyses, the sediments were stored in the lab overnight in a cold room at 0–4 °C and then sliced on the following day with a stainless steel knife that was cleaned after each cut. Sediments were sampled at 5 cm intervals to obtain sufficient material, at least 80 g per sample.

All granulometric and geochemical analyses were conducted at the national INRAE soil analyses facility in Arras, France, using the methods that are detailed on the facility's web site (www6.hautsdefrance.inrae.fr/las, accessed on 15 August 2022). Methods are summarized hereafter.

Sediments were first dried at 105 °C to determine their moisture content. For granulometry (standardised method: AFNOR X31 107), the organic matter (OM) content of sediments was removed using hot H_2O_2 after the solid material was crushed and sieved through meshes of 2 mm and 250 µm. Five fractions were measured in the granulometric analysis: clays ø<2 µm, fine silts 2–20 µm, coarse silts 20–50 µm, fine sands 50–200 µm, and coarse sands 200 µm-2 mm (calculated on the mineral sediment fraction). The coarse and fine fractions were obtained by sieving—dry sieving for coarse sands and wet sieving at 50 µm for fine sands after sampling the fine fractions (<50 µm), which were collected by performing three successive samplings with a "Robinson" pipette in a suspension of dry sediment with the addition of a dispersant. The organic matter (OM) content of sediments dried at 105 °C was measured by loss-on-ignition at 550 °C for 1 h. The residue was then heated to 1100 °C to determine the mineral matter (MM) content. The OM percentage of each sample was calculated as OM:(OM+MM)×100.

The measured elements were total nitrogen (N total), phosphorus (P_2O_5), potassium (K_2O), calcium (CaO), and magnesium (MgO), as well as the total and amorphous fractions of aluminium (Al) and iron (Fe), which were determined using the HF-$HClO_4$ method and the Tamm method respectively. Three MTE were also measured: cadmium (Cd), lead (Pb), and mercury (Hg).

Total nitrogen was measured by dry combustion in the presence of oxygen at 1000 °C, which transforms all the sediment N into gases N_2. After chromatographic separation, the total N was determined using a katharometer (method ISO 13878). Phosphorus (P) was extracted with $NaHCO_3$ buffered at pH 8.5, and its content was determined by spectrocolorimetry at 825 nm using the Olsen method (NF ISO 11263). K, Ca, and Mg were determined by the standard by argon-induced plasma (ICP-AES) and optical emission spectrometry methods after extraction with an ammonium acetate solution (pH 7).

The total Al and iron Fe fractions were measured using the HF-$HClO_4$ method. The amorphous fractions of Al, Fe, and silicon (SI) were measured using the Tamm method, which involves extraction with a solution of oxalic acid and ammonium oxalate (pH 3), in darkness at 20 °C followed by filtration. The elements of interest in the filtered extracts were then determined by spectrometry (ICP-AES).

Total Hg was determined using a dry combustion method (600 °C) under an oxygen flow. The released Hg is trapped by an amalgam and then released by heating to a high temperature for determination by atomic absorption spectrometry. Pb and Cd were measured simultaneously by mass spectrometry coupled with argon-induced plasma (ICP-MS).

3. Results

3.1. Sediment Profile and Chronology

The sediment between 90 and 82 cm was a gyttja, while that between 82 and 72 cm was a mixed gyttja–fibrous peat. From 72 cm upwards, the core exhibits no discontinuity and consisted mainly of a dense fibrous but decomposed blond peat of *Carex* that was rich in herb fibres and bryophytes (hypnaceae-type). The mean pH of the peat samples was 4.8 ± 0.3 (sd). Values were homogeneous along the core, except the two topmost samples that had the highest pH values: 5.2 at 5–10 cm, and 5.6 on the top core. The cationic exchange capacity was 41.4 ± 8.4 me.100 g^{-1}.

The radiocarbon dates were below 2000 years. The two topmost samples from the core (17–16 and 16–15 cm) had high corrected percent modern carbon (pMC) values, indicating that they consist of post-1950's sediments. The age–depth distribution of the radiocarbon measurements shows a classic pattern, with an apparent increase in the rate of peat accumulation at the top of the core (0 to 40 cm; see Table 1 and Figure 2) due to compaction and decomposition of peat deeper in the core (between 90 and 40 cm). Only one sample (taken at 66–67 cm) had a date inconsistent with the Bayesian model (1518 AD), being around 500 years younger than its expected age. Overall, the distribution indicates that the sediments below 70 cm are older than 500 AD, corresponding to the Roman epoch, with a peat inception phase dating to ca. 180 AD. The sediment between 70 to 65 cm date to the Middle Ages, those between 45 and 40 cm date to the modern period, and those above ca. 25 cm sediments are from the industrial era.

Table 1. Radiocarbon dating of the Caroux peat; all AMS measurements were conducted on decomposed plant fibres and bryophytes aside from the 86–87 cm sample, where the dated sediment was gyttja. Dating was performed at the LMC14 lab (Gif-sur-Yvette, France). Plant macroremains were extracted using hot KOH (7%) and sieved at 200 μm.

Depth (cm)	Lab. Code	Dated Dry Mass (mg)	Corrected Fraction of pMC	^{14}C Years	Calendar Years	Median Probability
15–16	SacA 16532	577	140.15 ± 0.36	n/a	Modern	n/a
16–17	SacA 16533	332	151.90 ± 0.30	n/a	Modern	n/a
32–33	SacA 16534	299	98.21 ± 0.25	145 ± 30 BP	1669–1947 AD	1812 AD
33–34	SacA 16535	390	99.38 ± 0.24	50 ± 30 BP	modern	
49–50	SacA 16536	491	98.21 ± 0.24	145 ± 30 BP	1669–1947 AD	1812 AD
50–51	SacA 16537	753	96.44 ± 0.26	290 ± 30 BP	1498–1792 AD	1565 AD
66–67	SacA 16538	667	95.50 ± 0.24	370 ± 30 BP	1451–1633 AD	1518 AD
67–68	SacA 16539	554	86.84 ± 0.23	1135 ± 30 BP	775–992 AD	926 AD
86–87	SacA 16540	2423	79.31 ± 0.22	1860 ± 30 BP	86–243 AD	179 AD

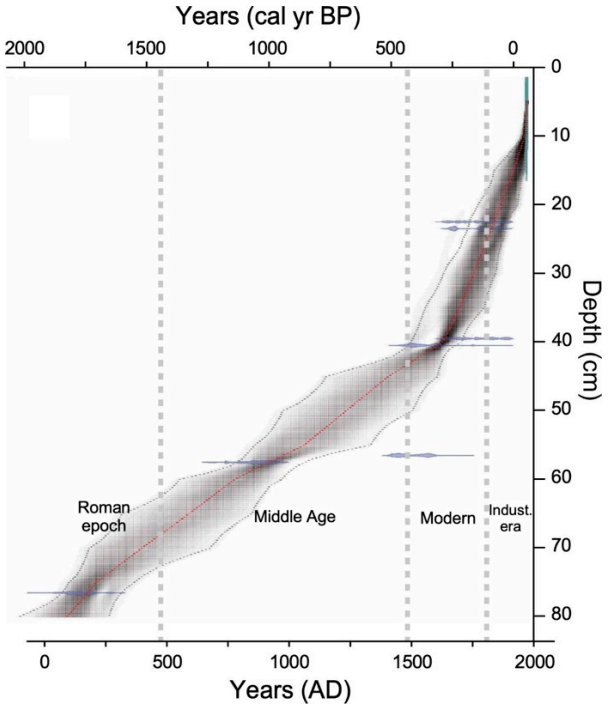

Figure 2. Depth distribution of radiocarbon measurements (violin plots), shown together with an age depth Bayesian model and the associated regional cultural chronology (bottom).

3.2. Granulometry, Organic Matter and Charcoal

The total mineral concentration of the sediment (dry weight) varied between 137 to 411 $mg \cdot g^{-1}$, (mean $\pm$sd: 250 $\pm$ 111 $mg \cdot g^{-1}$) with no discernible trend (not shown). Similarly, there were no apparent trends in the organic fraction (%; Figure 3). The granulometry was calculated based on the dry mass of mineral matter. The clay profile exhibited a slight but irregular increase in density, going from <400 $mg \cdot g^{-1}$ at the bottom to >500 $mg \cdot g^{-1}$ in the topmost cm ($r^2 = 0.56$, $p < 0.05$, Figure 3). No significant trends were detected in the silt and sand profiles (Figure 3). No charcoal was found, so no fire history reconstruction was possible.

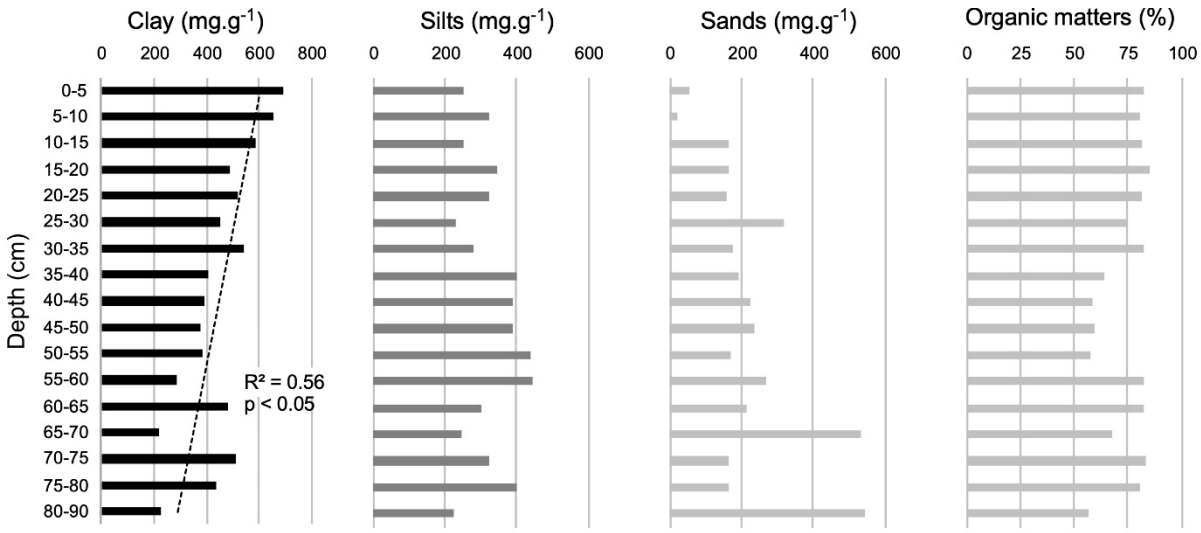

Figure 3. Concentration of clay, silts, and sands on the mineral matters fraction, and organic matter percentage inferred from loss-on-ignition at 550 °C. The dashed line represents a linear regression; the associated correlation and *p*-values are shown beside it.

3.3. Geochemistry

The nitrogen profile (total N) exhibited no discernible trend (Figure 4); the mean (±sd) N concentration was 17.0 ± 2.3 $mg_{total\text{-}N} \cdot g^{-1}$ (ranging from 12.4 $mg_{total\text{-}N} \cdot g^{-1}$ to 22.7 $mg_{total\text{-}N} \cdot g^{-1}$) and did not vary greatly with depth. The concentrations of phosphorous (P_2O_5), potassium (K_2O), calcium (CaO), and magnesium (MgO) all increased significantly ($p < 0.001$) from the bottom of the core without oscillation, following power functions for P_2O_5, K_2O, and CaO, and a logarithm function for MgO (Figure 4). This exponential increase begins at around 30–35 cm and, thus, coincides with the beginning of the industrial era (Figure 2).

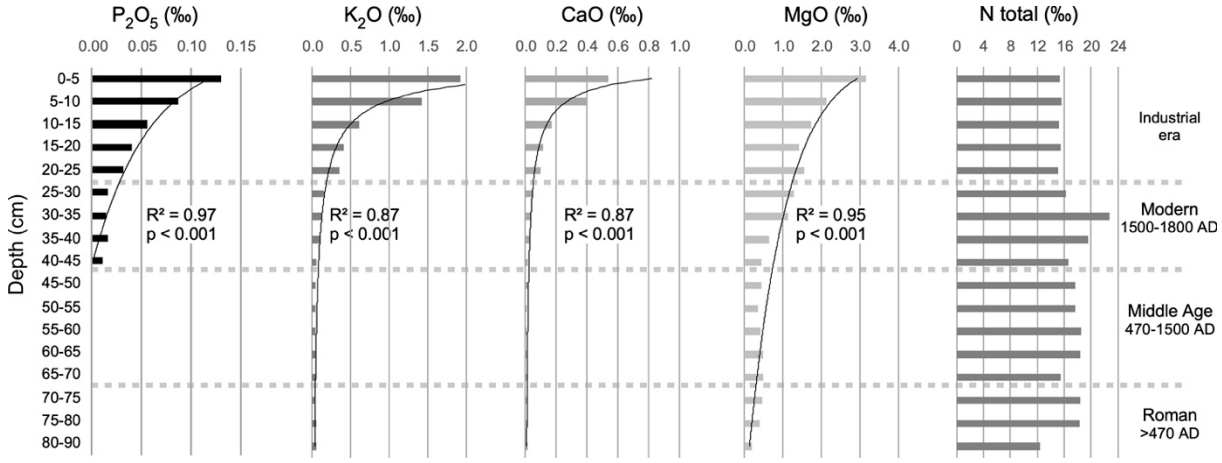

Figure 4. Concentration of phosphorous (P_2O_5), potassium (K_2O), calcium (CaO), magnesium (MgO), and nitrogen (N-total) as function of peat depth.

The total aluminium concentrations increase non-significantly with depth (not shown, $r^2 = 0.39$), while the concentration of amorphous aluminium increased significantly (Al-Tamm, $r^2 = 0.60$, $p < 0.01$; Figure 5a). In addition, the concentrations of both total iron (data not shown, $r^2 = 0.59$, $p < 0.01$) and amorphous iron form ($r^2 = 0.50$, $p < 0.05$; Figure 5b) increased significantly from the bottom to the top. The ratios of Al-Tamm and Fe-Tamm to the corresponding total concentrations are indicators of mineral weathering. The Al-Tamm:Al-tot ratio decreased sharply above 60 cm, suggesting that the rate of mineral weathering decreased in more recent times (Figure 5b), but no such pattern was seen for the Fe-Tamm:Fe-tot ratio (Figure 5e). However, the Fe-Tamm concentration increased with decreasing core depth (Figure 5d), similarly to the clay concentration (Figure 3). Fe-Tamm correlated well with the clay concentration ($r^2 = 0.60$, $p < 0.01$; Figure 5f), but the correlation was weaker for Fe-total ($r^2 = 0.27$, not significant), suggesting that the total load of amorphous Fe in the sediment is linked to the chemical weathering of clay inputs. The concentration of amorphous silicon (Si-Tamm) increased from the bottom to the top ($r^2 = 0.63$, $p < 0.01$; Figure 5c), indicating an increasing input of this element into the peat over time.

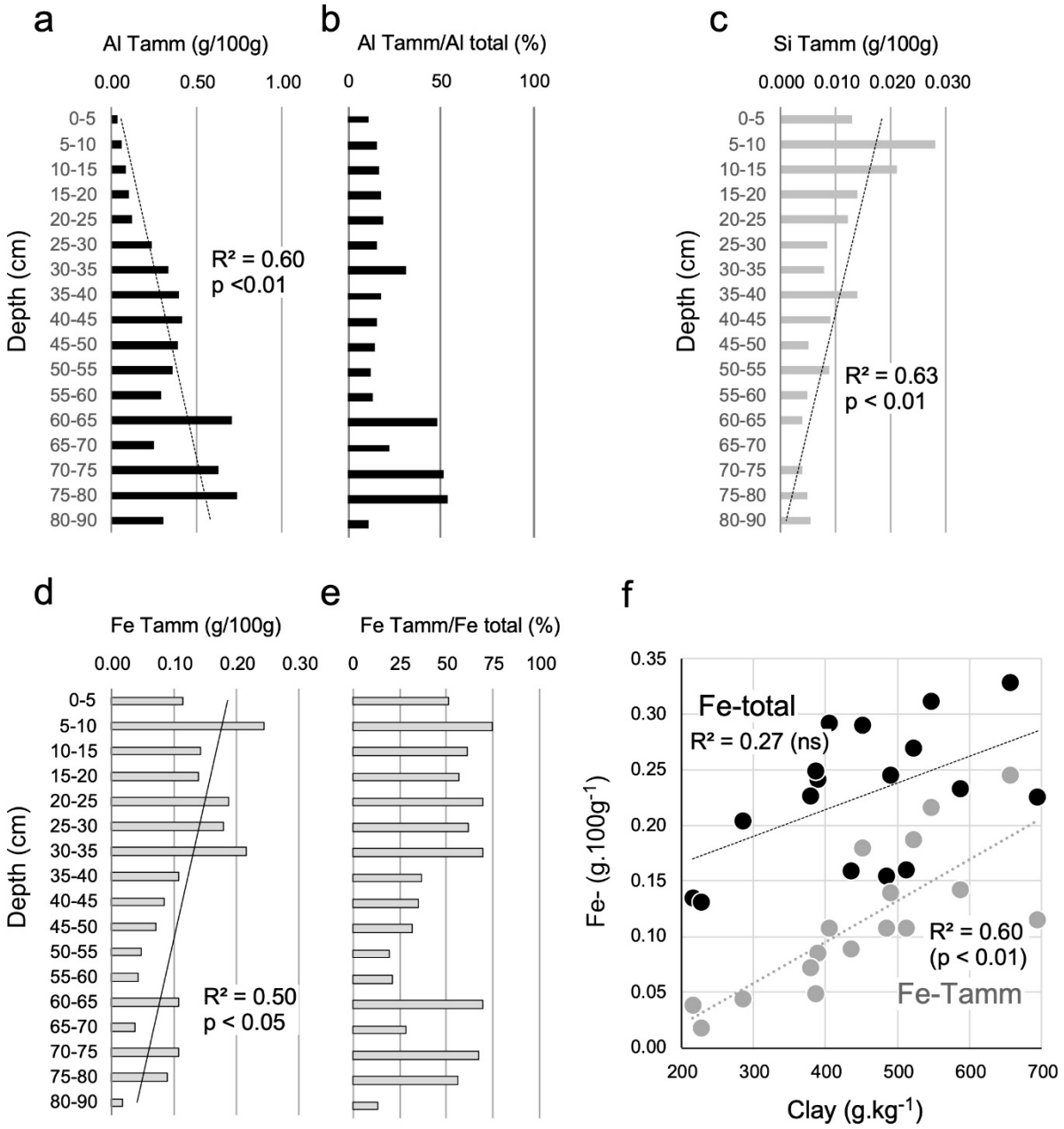

Figure 5. Aluminium (**a**,**b**), silicon (**c**) and iron (**d**,**e**) concentrations and amorphous:total ratios along the peat profile. For Al and Fe, the suffix -Tamm denotes the amorphous concentration (**a**,**d**). The ratio X-Tamm/X-total (**b**,**e**) reveals the contribution of the amorphous fraction of the metal (Al or Fe) to its total concentration (not shown). Concentrations of Fe-total and Fe-Tamm are plotted against the clay concentration (**f**) at the corresponding depth.

The MTE show different trends that are captured well by polynomials of order 6 (Cd $r^2 = 0.928$, $p < 0.001$, Hg $r^2 = 0.863$, $p < 0.001$), or 4 (Pb $r^2 = 0.938$, $p < 0.001$). While the cadmium (Cd) concentration is highest at the bottom of the profile (70–90 cm) and has a small peak at 35–30 cm, the lead (Pb) concentration is highest in the middle sediments, from 40 to 25 cm (Figure 6). Finally, mercury (Hg) concentration starts rising 40 cm from the top, reaching a maximum between 35 and 20 cm (Figure 6).

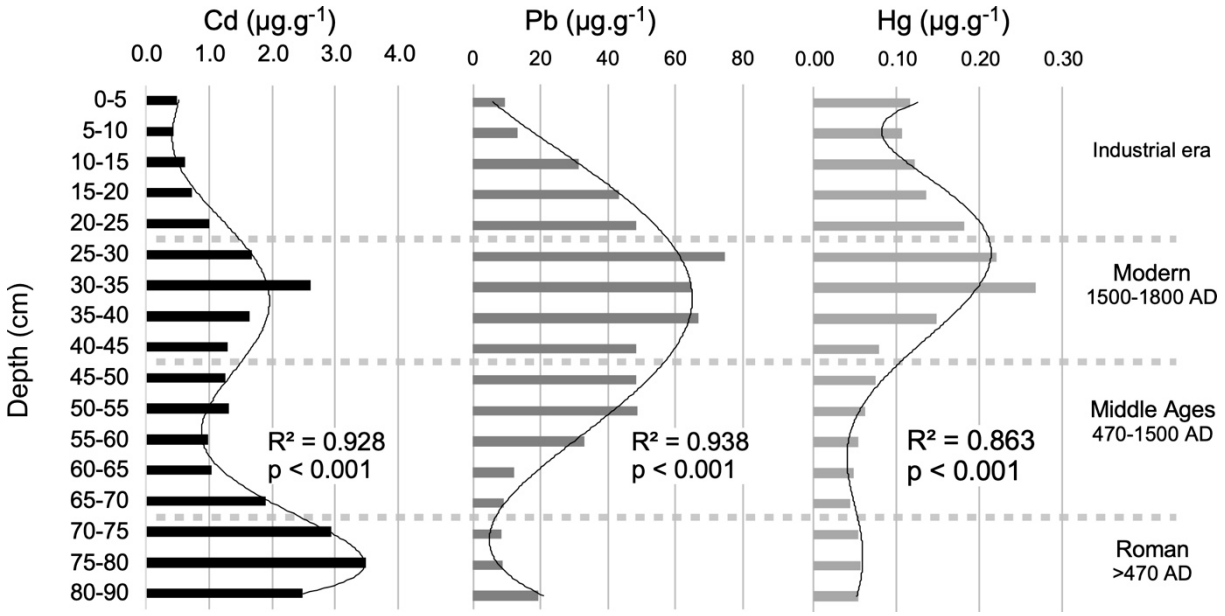

Figure 6. Concentration of the MTE cadmium (Cd), lead (Pb), and mercury (Hg) as function of peat depth.

4. Discussion

The chronology covers less than 2000 years, which is consistent with other regional studies on fens in the Mediterranean southeast Massif Central [25,29]. Despite a lack of charcoal particles, which made it impossible to perform wildfire reconstruction, the obtained geochemical and sedimentological results provide new insights into the functioning and environmental influences of the peat. The absence of charcoal raises several questions given that the studied site is Mediterranean and expected to burn periodically. The geochemical analyses suggested that the levels of metallic elements in the peat have been influenced by an array of different processes including bedrock weathering (aluminium), atmospheric particle deposition (clay, iron, and nutrients: Ca, Mg, K, P), and industrial activities leading to the deposition of MTE. These results are discussed in more detail below, starting with the surprising absence of charcoal.

4.1. Absence of Charcoal: No Wildfire Because of a Lack of Woody Cover

It is always difficult to interpret the lack of data, but it is very rare for charred particles to be absent from sediments, as demonstrated by the large numbers of reported charcoal series from all parts of the world, except the polar regions and deserts [30]. Charred particles are formed during fires, whose occurrence requires ignition (caused by lightning or human activities), suitable (dry) weather conditions, and fuel; the latter two factors control the fire spread [31,32]. Dry conditions favouring the fire spread are common in the Mediterranean regions: over the last 1850 years, there have been several dry periods of varying severity [33]. The main factor limiting the fire spread in this region is thus the availability of fuel, and woody cover in particular. If the plateau has remained without woody cover for the last 1900 years, grazing pressure by herds alone could explain the absence of wildfire. Similar absences of charcoal have been reported elsewhere in the Alps, for example in a fen over the last 1200 years [34] or in a peat from 4700 cal yr BP to the present [35]. In both cases, the lack of charcoal was associated with a lack of terrestrial woody macroremains, suggesting a long period of grassland cover without wildfires. A low frequency of fire over the last 2000 years on the granitic Mont Lozère (southwest of the Massif Central) that preceded the establishment of grasslands has been also observed [36], supporting a pollen-based analysis indicating that beech cover has disappeared, and grasslands have expanded since the end of the Middle Ages following

a 400-year period of wildfires [24]. Moreover, at a site with pine cover on the limestone steppe plateaux of the southern Massif Central, wildfires occurred only during an isolated 500-year period in the last 2000 years [37]. These records underscore the complexity of the regional chronology of forest wildfires over the past 2000 years. A common pattern is that all these areas were grassland dedicated to the raising of cattle of sheep, and that wildfires became rare or stopped completely once grasslands were established as already reported in the alps [34].

4.2. A Late Inception of Peat Accumulation

The finding that the peat at the studied site formed very recently (within the last 1900 years), could be due to climatic forcing or land use changes. Simple explanations based only on changing land use patterns seem reasonable at first glance. For example, earlier land uses might have removed the site's peat, as was previously observed in the Alps [35,38]. Second, anthropic deforestation could have reduced the evapotranspiration and thereby promoted OM accumulation and peat formation through paludification. Similar late peat formation processes associated with deforestation have been described elsewhere in the Massif Central [24,39,40], in Spain [25], Scotland [41], and also in Tasmania, where there was clear evidence that forest suppression had played a significant role in the process [42]. Ancient deforestation followed by the establishment of grasslands maintained by domestic herds is thus perhaps the most plausible explanation for the late Holocene peat formation driven by low evapotranspiration. However, a climate-driven scenario cannot be excluded, although this is not obvious from reconstructions showing a slightly oscillating climate from Roman times to the 20th century. Indeed, the last 2000 years were characterized by a relatively warm medieval period between 1000 and 1200 AD and a colder climate between 1500 and 1900 AD [43]. In addition, the periods between ca. 500 and 700 AD and between 1550 and 1850 AD [44] were comparatively wet. However, the most pronounced climatic change over the last 2000 years is the trend towards warming, with some years of extreme warmth and longer dryness that began in the late 20th century and continues today.

4.3. Local Processes Became Less Significant over time while Regional Influences Increased

The silicon concentration (Si) at the site increased as depth decreased (Figure 5c). This may have resulted from an increased supply of phytoliths to the peat due to an increase in the productivity of local herbs and sedges, particularly the *Molinia caerulea* currently present at the site. *Molinia* produce larger quantities of phytoliths than the dominant sedges [45]. However, it is more realistic to think that these increasing Si concentrations are linked to atmospheric inputs concomitant with clay inputs [46].

The trends in the concentration of amorphous aluminium (Al-Tamm, Figure 5a) support a scenario of a decrease in bedrock erosion and chemical weathering, which gradually produces less coarse particles and weakens the relationship between these processes and pedogenesis. As its thickness increases, the peat becomes less connected to the bedrock, and the ratio of amorphous to total aluminium (Al-Tamm:Al-total) decreases, probably because the amorphous material becomes increasingly complexed with organic matter, forming a secondary Al phase; organic-bound Al was not measured, but its concentration is estimated as the difference between the concentration of amorphous Al and total Al [3]. Consequently, a decrease in the proportion of amorphous Al along the core (Figure 5b), with no change in the total Al concentration (not shown), implies an increase in the concentration of organic-bound Al over time.

The clay concentrations also increased along the core (Figure 3), as did those of all nutrients other than nitrogen (Figure 4). The total iron (not shown) and amorphous iron (Fe-Tamm, Figure 5d) concentrations also both increased towards the upper end of the core, which is notable because they would be expected to behave like aluminium if changes in the abundance of iron were linked to local chemical weathering. However, because the amorphous iron concentration correlated well with that of clay (Figure 5f), it instead seems likely that atmospheric deposition was the main source of iron entering the peat.

The clay concentration is a proxy of aeolian activity, which delivers nutrients and iron contained in clay minerals to the peat. These clay inputs occurred throughout the last 1900 years but increased over the last two centuries in parallel with dramatic increases in the input of major agricultural nutrients (P and K). The depth profiles of N and P, K, Ca, and Mg differ, indicating that they were influenced by different processes. Nitrogen, which is recycled by biota, is homogeneously distributed across the peat depth, probably because it is sequestered in the organic matter [47]. In theory, P and K should also be sequestered in the OM, but P, K, Ca, and Mg can also be recycled or supplied by atmospheric inputs [47]. Their J-shaped depth profiles with high concentrations in the top sediments that decreased rapidly with increasing depth plead for recent atmospheric inputs. The hypothesis of a non-local supply of CaO and MgO is supported by the fact that the plateau's bedrock consists of Ca- and Mg-depleted granites and gneiss. The increase in the concentrations of CaO and MgO towards the top of the core (Figure 4), thus, indicates a strong contribution from regional or extra-regional aeolian processes—specifically, the deposition of airborne particles released by chemical weathering of calcareous soils. The main potential sources of CaO, MgO, P, and K are the rich Mediterranean lowlands (<200 m asl) a few km south of the Caroux plateau, which are farmed intensively. Human population growth in these regions and the associated increase in land use intensity over the last two centuries has probably accelerated lowland erosion, leading to airborne transport of the lightest mineral soil components (i.e., clay particles and the associated elements) to the plateau. However, atmospheric inputs of clay and elements can also come from extra-regional sources, notably from Africa during "red rain" events that transport Saharan dust [1], with significant contents of Ca, Mg, and K, to southern Europe [1,2,8].

4.4. Metal Trace Elements (MTE) Deposition

The MTE concentrations had two distinct modes within the core. The first was seen only for Cd and occurs in the deepest sediments corresponding to the Roman epoch while the second was seen for Pb, Hg and Cd during the modern period (1500–1800 AD). Hg concentrations remained high from the onset of the modern period through to the topmost sediments (Figure 6). These patterns could mirror regional mining activities, whose occurrence has been thoroughly documented by archaeological studies [15,16,48] and which have been shown to influence soil and sediment quality [17,24] in the region and elsewhere [2,4,5,7]. However, some of the Hg may have originated from biomass burning [18], the incidence of which peaked both globally and in the Mediterranean basin during the 19th century [49] after falling slightly over 2000 years [50].

Non-zero concentrations of Cd, Hg, and Pb were detected in all samples. This may reflect natural background levels of MTE originating from the bedrock [5,6,21,46,51], but these background levels can also be due to the atmospheric flux of anthropogenic pollution, resulting in a mixture of in situ (released from bedrock) and ex situ (pollution) processes [5,46]. The bedrock supported values are likely for Cd that presents high values peaking between 75–80 cm, i.e., in the deepest part of the peat profile. Cd is also considered to be mobile in peat [7], which may limit its usefulness as a proxy. However, the highest Cd concentration were here observed in the deepest sediments dated from the Roman period before AD 500 (Figure 6), in contrast to other studies where its concentration was highest in the uppermost sediments, typically deposited during the last 500 years. The latter pattern has been observed in places including Spain [19,20], southeast of the Massif Central [24], and northeastern France [22]. However, Cd has also a second peak at 30–35 cm that coincides with the Hg peak and the high values of Pb, two elements for which stratigraphical stability is not questioned [7,18]. This second Cd peak is dated from the modern period, i.e., between AD 1500 and 1800, which supports Spanish observations of inputs resulting from ore mining pollution during the last 500 years [19,20]. These different patterns raise questions about the mobility of Cd and its value as a sedimentological proxy that cannot be answered based on the results presented here; the Caroux chronology is too short to distinguish between the putative natural background and anthropic flux.

Increases in the concentration of Pb in peat beginning around 2500 years ago have been well documented in many European countries, and were linked to the activities of Greek, Celtic, or Roman civilisations [2,4,19,46]. However, the most pronounced reported increases in its concentration have occurred over the last 500 years [4,5,7,19]. In contrast, our record indicates a decrease in Pb inputs over the most recent decades, which could result from the public policies of phasing out lead gasoline in Europe during the late 20th century, although it actually happened in France in the year 2000 AD. The observed Hg concentrations are consistent with earlier reports showing that its accumulation peaked during the industrial era [52], although a regional shift may have begun during the Middle Ages [18].

Regional mining activities around the Caroux plateau during antiquity are well documented, particularly in the Montagne Noire massif and the lower Herault Valley to the east, where Fe was mined with silver and other metals for around 2500 years. Accordingly, several small mining and metallurgical workshops dating from the Middle Ages have been identified in this area [15,16,48], and more widely in the southern Massif Central [17]. This may explain the early increases in the concentrations of these elements on the plateau. Wood charcoal production, which was performed in all hills and mountains of the studied region from the Middle Ages to the 20th century [53,54], is likely to have been a major source of the atmospheric flux of Hg. Whatever, the sources of MTE and the chronology of their deposition, the results presented here clearly show that the minerotrophic peat of the Caroux plateau has been polluted by metallic deposits for at least 1900 years. Global warming and the spontaneous afforestation of the plateau combined with timber plantations could lead to decomposition of this peat, and, thus, a release of these pollutants, especially in cases of wildfires.

5. Conclusions

The minerotrophic peat of the Caroux plateau is no more than 1900 years old. Surprisingly, its sediments did not record the site's wildfire history, possibly due to a lack of woody communities at the site over at least the last 1900 years. This lack of trees and the resulting deficit of evapotranspiration may also be responsible for the peat's formation. However, it is also possible that wetter climatic episodes over the last 1900 years contributed to this process. The peat's geochemical composition appears to have been influenced much more heavily by atmospheric inputs than by local erosion and weathering processes, and the analyses revealed important inputs of air-transported light particles from the 18th century onwards, likely from the nearby calcareous agricultural plains of southern France (Languedoc). This aeolian process led to the deposition of clay, iron, and nutrients on the Caroux plateau, affecting the peat's trophic quality. Finally, both the peat and the plateau have been contaminated by a set of metallic trace elements. The peat's geochemistry has thus been influenced by regional mining, forestry, and agricultural activities, creating a strong social imprint. Collectively, these results reveal a long-standing human influence on the ecosystem of the Caroux that has existed for at least 1900 years and has become stronger over the last 200 years.

Author Contributions: V.G. conceived and designed the study; V.G. and C.C. realized all the samplings. V.G. carried out all the analyses. C.C. contributed to statistical analyses; V.G. and C.C. interpreted the results and wrote the manuscript. All authors have read and agreed to the published version of the manuscript.

Funding: This study was supported by the Institut des Sciences de l'Univers (CNRS, France) through the national program ARTEMIS for 14C dates (project PALEOFIRE, to CC).

Acknowledgments: We are thankful to Loic Birker and Brice Mourier for their help during fieldwork, to Loic Bircker for his contribution for the charcoal analysis, and to Bérangère Leys for her help with the Bayesian age/depth model. The English text was edited with SEES-Editing Ltd.

Conflicts of Interest: The authors declare no conflict of interest.

References

1. Loÿe-Pilot, M.D.; Martin, J.M.; Morelli, J. Influence of Saharan dust on the rain acidity and atmospheric input to the Mediterranean. *Nature* **1986**, *321*, 427–428. [CrossRef]
2. Cortizas, A.M.; López-Costas, O.; Orme, L.; Mighall, T.; Kylander, M.E.; Bindler, R.; Sala, G. Holocene atmospheric dust deposition in NW Spain. *Holocene* **2019**, *30*, 507–518. [CrossRef]
3. Mourier, B.; Poulenard, J.; Chauvel, C.; Faivre, P.; Carcaillet, C. Distinguishing subalpine soil types using extractible Al and Fe fractions and REE geochemistry. *Geoderma* **2008**, *145*, 107–120. [CrossRef]
4. Renberg, I.; Persson, M.W.; Emteryd, O. Pre-industrial atmospheric lead contamination detected in Swedish lake sediments. *Nature* **1994**, *368*, 323–326. [CrossRef]
5. Shotyk, W.; Cheburkin, A.K.; Appleby, P.G.; Fankhauser, A.; Kramers, J.D. Two thousand years of atmospheric arsenic, antimony, and lead deposition recorded in an ombrotrophic peat bog profile, Jura Mountains, Switzerland. *Earth Planet. Sci. Lett.* **1996**, *145*, E1–E7. [CrossRef]
6. Rausch, N.; Nieminen, T.; Ukonmaanaho, L.; Le Roux, G.; Krachler, M.; Cheburkin, A.K.; Bonani, G.; Shotyk, W. Comparison of Atmospheric Deposition of Copper, Nickel, Cobalt, Zinc, and Cadmium Recorded by Finnish Peat Cores with Monitoring Data and Emission Records. *Environ. Sci. Technol.* **2005**, *39*, 5989–5998. [CrossRef]
7. Allan, M.; Le Roux, G.; De Vleeschouwer, F.; Bindler, R.; Blaauw, M.; Piotrowska, N.; Sikorski, J.; Fagel, N. High-resolution reconstruction of atmospheric deposition of trace metals and metalloids since AD 1400 recorded by ombrotrophic peat cores in Hautes-Fagnes, Belgium. *Environ. Pollut.* **2013**, *178*, 381–394. [CrossRef]
8. Loye-Pilot, M.D.; Morelli, J. Flucturations of ionic composition of precipitations collected in Corsica related to changes in the origins of incoming aerosols. *J. Aerosol. Sci.* **1988**, *19*, 577–585. [CrossRef]
9. Carcaillet, C.; Bouvier, M.; Fréchette, B.; Larouche, A.C.; Richard, P.J. Comparison of pollen-slide and sieving methods in lacustrine charcoal analyses for local and regional fire history. *Holocene* **2001**, *11*, 467–476. [CrossRef]
10. Clark, J.S.; Lynch, J.; Stocks, B.J.; Goldammer, J.G. Relationships between charcoal particles in air and sediments in west-central Siberia. *Holocene* **1998**, *8*, 19–29. [CrossRef]
11. Ohlson, M.; Tryterud, E. Interpretation of the charcoal record in forest soils: forest fires and their production and deposition of macroscopic charcoal. *Holocene* **2000**, *10*, 519–525. [CrossRef]
12. Lynch, J.A.; Clark, J.S.; Stocks, B.J. Charcoal production, dispersal, and deposition from the Fort Providence experimental fire: interpreting fire regimes from charcoal records in boreal forests. *Can. J. For. Res.* **2004**, *34*, 1642–1656. [CrossRef]
13. Brun, J.-P.; Laubenheimer, F. Conclusion. *Gallia* **2001**, *58*, 203–219. [CrossRef]
14. Laubenheimer, F. (Ed.) *20 ans de Recherches à Sallèle d'Aude*; Institut des Sciences et Techniques de l'Antiquité (Collection ISTA, 760), Presses Universitaires Franc-Comtoises: Besançon, France, 2001; p. 302.
15. Decombeix, P.M.; Domergue, C.; Fabre, J.-M.; Gorgues, A.; Rico, C.; Tollon, F.; Tournier, B. Réflexions sur l'organisation de la production de fer à l'époque romaine dans le bassin supérieur de la Dure, au voisinage des Martys (Aude). *Gallia* **2002**, *57*, 23–36. [CrossRef]
16. Beyrie, A.; Fabre, J.M.; Kammenthaler, E.; Mantenant, J.; Munteanu, G.; Rico, C. Une vaste exploitation minière du second Âge du fer. La mine de cuivre des Barrencs (Lastours, Fournes-Cabardès, Aude). *Rev. Archéologique De La Narbonn.* **2011**, *44*, 39–55. [CrossRef]
17. Baron, S.; Carignan, J.; Laurent, S.; Ploquin, A. Medieval lead making on Mont-Lozère Massif (Cévennes-France): Tracing ore sources using Pb isotopes. *Appl. Geochem.* **2006**, *21*, 241–252. [CrossRef]
18. Enrico, M.; Le Roux, G.; Heimbürger, L.-E.; Van Beek, P.; Souhaut, M.; Chmeleff, J.; Sonke, J.E. Holocene Atmospheric Mercury Levels Reconstructed from Peat Bog Mercury Stable Isotopes. *Environ. Sci. Technol.* **2017**, *51*, 5899–5906. [CrossRef]
19. Martinez-Cortizas, A.; Pontevedra Pombal, X.; Novoa Munoz, J.C.; Garcia-Rodeja, E. Four thousand years of atmospheric Pb, Ca and Zn deposition recorded by the ombrotrophic peat bog of Penido Vello (Northwestern Spain). *Water Air Soil Pollut.* **1997**, *100*, 387–403. [CrossRef]
20. Pontevedra-Pombal, X.; Mighall, T.M.; Nóvoa-Muñoz, J.C.; Peiteado-Varela, E.; Rodríguez-Racedo, J.; García-Rodeja, E.; Martínez-Cortizas, A. Five thousand years of atmospheric Ni, Zn, As, and Cd deposition recorded in bogs from NW Iberia: prehistoric and historic anthropogenic contributions. *J. Archaeol. Sci.* **2013**, *40*, 764–777. [CrossRef]
21. Bindler, R.; Rydberg, J.; Renberg, I. Establishing natural sediment reference conditions for metals and the legacy of long-range and local pollution on lakes in Europe. *J. Paleolimnol.* **2010**, *45*, 519–531. [CrossRef]
22. Mariet, A.-L.; Monna, F.; Gimbert, F.; Bégeot, C.; Cloquet, C.; Belle, S.; Millet, L.; Rius, D.; Walter-Simonnet, A.-V. Tracking past mining activity using trace metals, lead isotopes and compositional data analysis of a sediment core from Longemer Lake, Vosges Mountains, France. *J. Paleolimnol.* **2018**, *60*, 399–412. [CrossRef]
23. Carcaillet, C.; Perroux, A.-S.; Genries, A.; Perrette, Y. Sedimentary charcoal pattern in a karstic underground lake, Vercors massif, French Alps: implications for palaeo-fire history. *Holocene* **2007**, *17*, 845–850. [CrossRef]
24. Vives, G.S.; Miras, Y.; Riera, S.; Julià, R.; Allée, P.; Orengo, H.; Paradis-Grenouillet, S.; Palet, J.M. Tracing the land use history and vegetation dynamics in the Mont Lozère (Massif Central, France) during the last 2000 years: The interdisciplinary study case of Countrasts peat bog. *Quat. Int.* **2014**, *353*, 123–139. [CrossRef]

25. Pontevedra-Pombal, X.; Castro, D.; Carballeira, R.; Souto, M.; López-Sáez, J.; Pérez-Díaz, S.; Fraga, M.; Valcárcel, M.; García-Rodeja, E. Iberian Acid Peatlands: Types, Origin and General Trends of Development. 2017, pp. 1–19. Available online: https://digital.csic.es/bitstream/10261/199953/4/iberian_acid_peatlands.pdf (accessed on 18 August 2022).
26. Stuiver, M.; Reimer, P.J. Extended 14C data base and revised CALIB 3.0 14C age calibration program. *Radiocarbon* **1993**, *35*, 215–230. [CrossRef]
27. Reimer, P.J.; Austin, W.E.N.; Bard, E.; Bayliss, A.; Blackwell, P.G.; Ramsey, C.B.; Butzin, M.; Cheng, H.; Edwards, R.L.; Friedrich, M.; et al. The IntCal20 Northern Hemisphere Radiocarbon Age Calibration Curve (0–55 cal kBP). *Radiocarbon* **2020**, *62*, 725–757. [CrossRef]
28. Blaauw, M.; Christen, J.A. Flexible paleoclimate age-depth models using an autoregressive gamma process. *Bayesian Anal.* **2011**, *6*, 457–474. [CrossRef]
29. Bottollier-Curtet, M.; Muller, S. Dynamique et context passes du développement d'une tourbière méditerranéenne (Massif de l'Aigoual, France). *C. R. Biol.* **2009**, *332*, 69–82. [CrossRef]
30. Power, M.J.; Marlon, J.; Ortiz, N.; Bartlein, P.J.; Harrison, S.P.; Mayle, F.E.; Ballouche, A.; Bradshaw, R.H.W.; Carcaillet, C.; Cordova, C.; et al. Changes in fire regimes since the Last Glacial Maximum: an assessment based on a global synthesis and analysis of charcoal data. *Clim. Dyn.* **2007**, *30*, 887–907. [CrossRef]
31. Pausas, J.G.; Fernández-Muñoz, S. Fire regime changes in the Western Mediterranean Basin: from fuel-limited to drought-driven fire regime. *Clim. Chang.* **2011**, *110*, 215–226. [CrossRef]
32. Fréjaville, T.; Curt, T.; Carcaillet, C. Tree cover and seasonal precipitation drive understorey flammability in alpine mountain forests. *J. Biogeogr.* **2016**, *43*, 1869–1880. [CrossRef]
33. Trouet, V.; Panayotov, M.; Ivanova, A.; Frank, D. A pan-European summer teleconnection mode recorded by a new temperature reconstruction from the northeastern Mediterranean (ad 1768–2008). *Holocene* **2012**, *22*, 887–898. [CrossRef]
34. Genries, A.; Muller, S.D.; Mercier, L.; Bircker, L.; Carcaillet, C. Fires control spatial variability of subalpine vegetation dynamics during the Holocene in the Maurienne valley (French Alps). *Écoscience* **2009**, *16*, 13–22. [CrossRef]
35. Oris, F.; Lamentowicz, M.; Genries, A.; Mourier, B.; Blarquez, O.; Ali, A.A.; Bremond, L.; Carcaillet, C.; Mariusz, L. Holocene changes in climate and land use drove shifts in the diversity of testate amoebae in a subalpine pond. *J. Paleolimnol.* **2013**, *49*, 633–646. [CrossRef]
36. Bal, M.C.; Allée, P.; Liard, M. Charcoal from soil: The origin of Nardus stricta grassland and the history of a mountain cultural landscape (Mont Lozère, France) since the Neolithic period. *Quat. Int.* **2015**, *366*, 3–14. [CrossRef]
37. Vernet, J.-L. History of the Pinus sylvestris and Pinus nigra ssp. salzmanni forest in the Sub-Mediterranean mountains (Grands Causses, Saint-Guilhem-le-Désert, southern Massif Central, France) based on charcoal from limestone and dolomitic deposits. *Veg. Hist. Archaeobotany* **2006**, *16*, 23–42. [CrossRef]
38. Coûteaux, M. Recherches pollenanalytiques en Oisans: Le plateau de Brande (Alpe d'Huez, Isere, France). *Bull. Soc. R. Bot. Belgique* **1982**, *115*, 91–106.
39. Cubizolle, H.; Tourman, A.; Argant, J.; Porteret, J.; Oberlin, C.; Serieyssol, K. Origins or European biodiversity: paleo-geographic signification of peat inception during the Holocene in. the granitic eastern Massiff Central (France). *Landsc. Ecol.* **2003**, *18*, 227–238. [CrossRef]
40. Cubizolle, H.; Fassion, F.; Argant, J.; Latour-Argant, C.; Galet, P.; Oberlin, C. Mire initiation, climatic change and agricultural expansion over the course of the Late-Holocene in the Massif Central mountain range (France): causal links and implication for mire conservation. *Quat. Intern.* **2012**, *251*, 77–96. [CrossRef]
41. Frenzel, B. L'Homme comme facteur géologique en Europe. *Bull. Asso. Française Etude Quat.* **1979**, *16*, 191–199. [CrossRef]
42. Fletcher, M.-S.; Wood, S.W.; Haberle, S.G. A fire-driven shift from forest to non-forest: evidence for alternative stable states? *Ecology* **2014**, *95*, 2504–2513. [CrossRef]
43. Lüning, S.; Schulte, L.; Garcés-Pastor, S.; Danladi, I.; Gałka, M. The Medieval Climate Anomaly in the Mediterranean Region. *Paleoceanogr. Paleoclimatol.* **2019**, *34*, 1625–1649. [CrossRef]
44. Cisneros, M.; Cacho, I.; Moreno, A.; Stoll, H.; Torner, J.; Català, A.; Edwards, R.L.; Cheng, H.; Fornós, J.J. Hydroclimate variability during the last 2700 years based on stalagmite multi-proxy records in the central-western Mediterranean. *Quat. Sci. Rev.* **2021**, *269*, 107137. [CrossRef]
45. Klančnik, K.; Vogel-Mikuš, K.; Gaberščik, A. Silicified structures affect leaf optical properties in grasses and sedge. *J. Photochem. Photobiol. B Biol.* **2014**, *130*, 1–10. [CrossRef]
46. Weiss, D.; Shotyk, W.; Cheburkin, A.K.; Gloor, M.; Reese, S. Atmospheric Lead Deposition from 12,400 to ca. 2000 yrs BP in a Peat Bog Profile, Jura Mountains, Switzerland. *Water Air Soil Pollut.* **1997**, *100*, 311–324. [CrossRef]
47. Verhoeven, J.T.A. Nutrient dynamics in minerotrophic peat mires. *Aquat. Bot.* **1986**, *25*, 117–137. [CrossRef]
48. Carozza, L.; Georjon, C. La fin du Néolithique et les débuts de la métallurgie en Languedoc central: contrôle social du territoire et pratiques économiques entre 3200 et 2400 av. J.-C. dans la moyenne vallée de l'Hérault. *Rev. Archéologique De L'est* **2006**, *25*, 215–237.
49. Marlon, J.R.; Bartlein, P.J.; Daniau, A.-L.; Harrison, S.P.; Maezumi, S.Y.; Power, M.J.; Tinner, W.; Vanniére, B. Global biomass burning: A synthesis and review of Holocene paleofire records and their controls. *Quat. Sci. Rev.* **2013**, *65*, 5–25. [CrossRef]
50. Marlon, J.; Bartlein, P.; Carcaillet, C.; Gavin, D.; Harrison, S.; Higuera, P.; Joos, F.; Power, M.J.; Prentice, I.C. Climate and human influences on global biomass burning over the past two millennia. *Nat. Geosci.* **2008**, *1*, 697–702. [CrossRef]

51. Talbot, J.; Moore, T.R.; Wang, M.; Dallaire, C.O.; Riley, J.L. Distribution of lead and mercury in Ontario peatlands. *Environ. Pollut.* **2017**, *231*, 890–898. [CrossRef]
52. Allan, M.; Le Roux, G.; Sonke, J.E.; Piotrowska, N.; Streel, M.; Fagel, N. Reconstructing historical atmospheric mercury deposition in Western Europe using: Misten peat bog cores, Belgium. *Sci. Total Environ.* **2013**, *442*, 290–301. [CrossRef]
53. Fabre, L. Le Charbonnage Historique de la Chênaie à Quercus Ilex L. (Languedoc, France): Conséquences Écologiques. Ph.D. Thesis, University of Montpellier 2, Montpellier, France, 1996.
54. Allée, P.H.; Paradis, S.; Boumedienne, F. La forêt médiévale charbonnée du Mont Lozère: de la paléométallurgie à l'archéologie forestière. *Archéosciences* **2010**, *34*, 177e186.